Journal of Materials Chemistry A

Accepted Manuscript

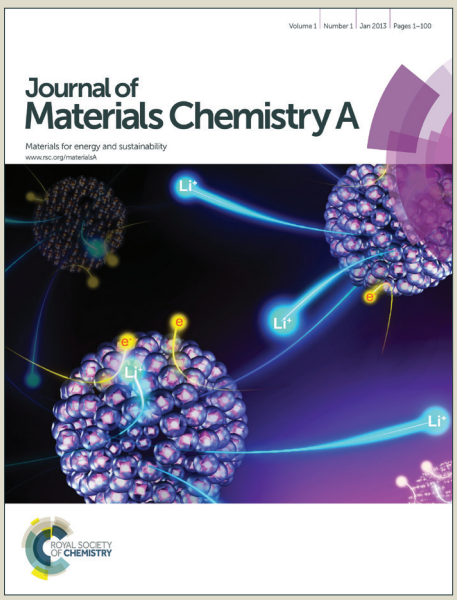

ROYAL SOCIETY OF CHEMISTRY

www.rsc.org/materialsA

Energy & Environmental Science

Journal of Materials Chemistry A

Dynamic Article Links ►

Cite this: DOI: 10.1039/c0xx00000x

ARTICLE TYPE

www.rsc.org/xxxxxx

$Li_xV_2O_5/LiV_3O_8$ nanoflakes with significantly improved electrochemical performance for Li-ion batteries

Dan Sun[a], Guanhua Jin[a], Haiyan Wang[a]*, Xiaobing Huang[b], Yu Ren[c], Jiecao Jiang[a], Hanna He[a] and Yougen Tang[a]

Received (in XXX, XXX) Xth XXXXXXXXX 20XX, Accepted Xth XXXXXXXXX 20XX
DOI: 10.1039/b000000x

Abstract**:** Poor cycling stability and rate capability are the main challenges for LiV_3O_8 as the cathode material for Li-ion battery. Here a novel strategy involving the self-transformation of superficial LiV_3O_8 in reducing atmosphere (H_2/Ar) was reported to fabricate $Li_xV_2O_5/LiV_3O_8$ nanoflakes. X-ray diffraction (XRD), X-ray photoelectron spectroscopy (XPS) and high resolution transmission electron microscopy (HRTEM) results demonstrate that $Li_xV_2O_5/LiV_3O_8$ nanoflakes could be in-situ formed and the thickness of $Li_xV_2O_5$ layer is controllable. When used as a cathode for Li-ion battery, $Li_xV_2O_5/LiV_3O_8$ nanoflakes exhibit significantly improved cycling stability with the capacity retention of *ca.* 82% over 420 cycles at 1C-rate (1C = 300 $mA\cdot g^{-1}$), and much better rate performance compared with bare LiV_3O_8. The improvement of electrochemical performance should be attributed to the unique core-shell structure, in which the ultrathin $Li_xV_2O_5$ layer could not only protect the internal LiV_3O_8 from dissolution, but also increase the Li ions diffusion coefficient and suppress the charge-transfer resistance, as verified by electrochemical impedance spectroscopy (EIS) and XRD results.

Introduction

Li-ion batteries (LIBs) have drawn more and more attention due to their wide applications in portable electronics and the great potential for powering electric vehicles (EVs) and large-scale stationary energy storage[1, 2]. However, current commercial lithium ion batteries, which mostly rely on lithium transition metal oxides ($LiCoO_2$, $LiMn_2O_4$, $LiNi_{1/3}Co_{1/3}Mn_{1/3}O_2$, *etc*.) as cathodes, are hard to fulfill the future requirement for high energy storage. Therefore, developing new alternative materials with higher energy and power density is of great urgency. Vanadium oxides and their derivatives are receiving a great deal of interest as cathode candidates for LIBs owing to their high reversible capacity, ease of fabrication and low cost[3, 4]. Among them, LiV_3O_8 is the most studied one. It is noted that as-prepared approaches and the following heat treatment greatly influence the electrochemical performance. With this regard, a number of methodologies (improved solid state reaction[5, 6], sol-gel method[7-11], hydrothermal synthesis[12], microwave-assisted synthesis[13, 14], spray-drying method[4, 15] *etc*.) have been developed. However, its inferior cycling stability and rate performance are still the main challenges for the further application[11, 12]. Gu *et al.*[16] reported 1D arrays of LiV_3O_8 with a high initial discharge capacity of 352 $mAh\cdot g^{-1}$, but it decreased drastically to 255 $mAh\cdot g^{-1}$ after 40 cycles. Single-crystalline LiV_3O_8 nanorods[6] exhibited the reversible capacities of 348 $mAh\cdot g^{-1}$ at 20 $mA\cdot g^{-1}$ but only 200 $mAh\cdot g^{-1}$ at 100 $mA\cdot g^{-1}$.

Unstable crystal structure (irreversible phase transformation[17, 18] and dissolution of vanadium[19]) is considered to be the main reason of capacity fading, while the intrinsic slow Li^+ kinetic diffusion between the layers in LiV_3O_8 is believed to be responsible for the inferior rate capability[20]. Therefore, strategies should be employed to further improve the cycling stability and rate performance. Surface modification with conducting materials, appears to be efficient to enhance electrochemical properties of LiV_3O_8 via suppressing the dissolution of active materials and the overall phase change[3]. There have been some papers involving the surface modifications (carbon[21], polyaniline (PAn)[3, 22], $AlPO_4$[23], AlF_3[24], Al_2O_3[25] *etc*) for LiV_3O_8. Although the cycling stability could be improved, the reversible capacity of LiV_3O_8 decreased because the coating material is non-active and it probably brings forth structural variation. It has been verified that V^{5+} in LiV_3O_8 is susceptible to the coating material during the high-temperature sintering process. The discharge capacity of LiV_3O_8 decreased from 335 $mAh\cdot g^{-1}$ to 227 $mAh\cdot g^{-1}$ after carbon coating[21] and from 283 $mAh\cdot g^{-1}$ to 243 $mAh\cdot g^{-1}$ after PAn[22] coating. How to achieve the uniform coating layer on LiV_3O_8 by an in-situ strategy is still a big challenge for significant improvement of electrochemical properties[26, 27].

Herein, we first propose a novel in-situ transformation method to fabricate $Li_xV_2O_5$ coated LiV_3O_8 nanoflakes. It is known that $Li_xV_2O_5$ owns a much higher Li ion diffusion coefficient (~10^{-10} $cm^2\cdot s^{-1}$)[28] than LiV_3O_8 (~10^{-13} $cm^2\cdot s^{-1}$).[29] In spite of inferior cycling stability, $Li_xV_2O_5$ is also a good cathode candidate for Li-ion battery. Thus a proper thickness of $Li_xV_2O_5$ layer seems to be beneficial to electrochemical interfacial properties of LiV_3O_8 at the expense of minimum capacity loss. In the present work, $Li_xV_2O_5/LiV_3O_8$ nanoflakes were simply formed by treating the LiV_3O_8 nanoflakes in reduction atmosphere (H_2/Ar mixed gas). The favorable merits of this in-situ transformation strategy are expected to be achieved: (1) the outside $Li_xV_2O_5$ layer is very

uniform and the combination between $Li_xV_2O_5$ and LiV_3O_8 is much closer than other common coating method, probably resulting in superior stability during the Li ion insertion/ extraction process; (2) the thickness of $Li_xV_2O_5$ layer could be well controlled by the variation of treating time. When used as a cathode material for Li ion battery, $Li_xV_2O_5/LiV_3O_8$ nanoflakes exhibit much better cycling stability (*ca.* 82% over 420 cycles) and rate capability in comparison with the bare LiV_3O_8. This novel in-situ transformation strategy can be extended to other kinds of electrode materials for surface modification.

Experimental

Synthesis of LiV_3O_8

All the starting materials were analytically pure grade and used directly without any purification. A typical hydrothermal method was employed to prepare $(NH_4)_{0.5}V_2O_5$ precursor. Oxalic acid (2.28 g, 99.5%, Sinopharm Chemical Reagent Co., Ltd.) and NH_4VO_3 (2.55 g, 99%, Tianjin Guangfu Institute of Fine Chemicals) were first dissolved in distilled water with rapid stirring. Then, the yellow-green solution was transferred into a 100 ml Teflon lined stainless steel autoclave. The autoclave was sealed and heated at 180 °C for 12 h. After that, the autoclave was cooled down to room temperature naturally. The precipitate was filtered, washed with distilled water several times and then dried at 80 °C overnight. Following that, a proper amount of $(NH_4)_{0.5}V_2O_5$ was added into lithium hydroxide (Tianjin Institute of Chemical Reagents) solution (the molar ratio of Li: V in theory is 1: 3). 0.2 g of PEG4000 was used as dispersing agent. The mixture was stirred for 2 h at room temperature and then heated at 80 °C in a hotplate under stirring to evaporate the distilled water. The collected powder was sintered at 450 °C for 8 h in air to obtain the LiV_3O_8 (marked as LVO).

Synthesis of $Li_xV_2O_5/LiV_3O_8$ composite

The as-prepared LiV_3O_8 was put into the tube furnace, after feeding Ar gas for 30 min with a flow rate of 100 cm^3/min, the temperature was increased to 450 °C with a ramping rate of 15 °C/min. Then, the Ar flow was switched to 5% H_2/Ar flow with the flow rate of 60 cm^3/min for 1, 5, 10, 30 min, respectively (the corresponding as-prepared products were marked as LVO-1, LVO-5, LVO-10, LVO-30). Once the annealing time was over, the furnace was powered off and the feeding gas was stopped immediately. The tube furnace was cooled to room temperature naturally.

Characterizations

X-ray diffraction (XRD) data were examined by the X-ray diffractometer (DX-2700, Dandong Haoyuan) utilizing a Cu-Kα1 source with a step of 0.02°. For the XRD test of cycled electrode, the cells were first disassembled and the electrodes were soaked in dimethyl carbonate (DMC) for 1 h and then rinsed several times with DMC to remove the electrolyte. Then the electrode film consisting of active material, Super P carbon and polytetrafluoroethylene (PTFE) pressed on the stainless steel mesh was treated under vaccum to remove the residual DMC. The related operations were carried out in an Ar-filled MBraun glove box. Finally, the whole electrode was used to examine the XRD test and no obvious signal of stainless steel mesh was observed probably due to the thick electrode film.

X-ray photoelectron spectroscopy (XPS) measurement was performed on the K-Alpha1063 spectrometer. The XPS patterns were collected using Al Kα radiation at a voltage of 12 kV and current of 6 mA. Charging effect was corrected by adjusting the binding energy of C1s peak from carbon contamination to 284.5 eV. Morphological studies were conducted using a Nova NanoSEM 230 scanning electron microscopy (SEM) and a JEOL JEM-2100F transmission electron microscopy (TEM) employing a LaB6 filament as the electron source and an accelerating voltage of 200 keV. The high resolution TEM (HRTEM) images were also obtained from JEOL JEM-2100F transmission electron microscopy.

Electrochemical measurements

The electrodes were fabricated by mixing the active material, polyvinylidene fluoride (PVDF), and Super P carbon in a weight ratio of 80: 10:10 using tetrahydrofuran (THF) as solvent. The mixture was stirred for 6 h and then cast onto the Al foil. After solvent evaporation at room temperature, the electrodes were dried at 110 °C under vacuum for 12 h. The loading mass of each electrode ranges from 1.5 to 2.5 mg cm^{-2}. The construction of electrodes after different cycles for ex-situ XRD testing is different from that for electrochemical measurement since some of powder in electrode after cycling tends to exfoliate. To address this issue, the electrodes were fabricated by pressing a mixture of the active material, Super P carbon, and PTFE in a weight ratio of 80:10:10 using distilled water as solvent on a stainless steel mesh collector at 20 MPa firstly and then dried at 110 °C under vacuum for 8 h. The electrodes were assembled into CR2016 coin-type cells with commercial electrolyte (Guangzhou Tinci Materials Technology Co., Ltd; 1 M $LiPF_6$ in 1:1 v/v ethylene carbonate/ dimethyl carbonate) and a Li metal as counter electrode. The cells were constructed in an Ar-filled MBraun glovebox and then cycled galvanostatically between 1.5 and 4.0 V (versus Li^+/Li) at a desired current density using a Neware battery testing system (CT-3008W) at room temperature. Cyclic voltammetry (CV) test was carried out using the CHI 660c electrochemical station (Shanghai Chenhua, China) with a scan rate of 0.1 $mV \cdot s^{-1}$ at room temperature. Electrochemical impedance spectroscopy (EIS) was recorded by a Princeton workstation (PARSTAT2273, EG&G, US) over the frequency range from 500 kHz to 10 mHz with an amplitude of 5 mV. Before EIS test, the cells were charged to 2.8 V and then kept at that voltage for a period of time to reach a stable state.

Results and discussion

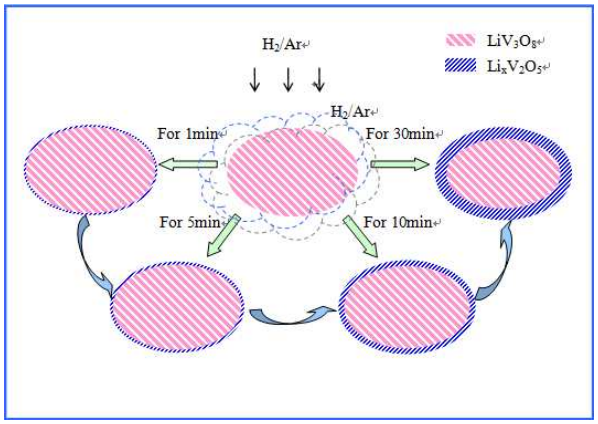

Fig. 1 The schematic illustration of the formation for $Li_xV_2O_5/LiV_3O_8$ composite.

The schematic illustration of formation mechanism for $Li_xV_2O_5/LiV_3O_8$ composite is proposed in Fig. 1. When heated in H_2/Ar (5%), superficial LiV_3O_8 would be partially reduced to

$Li_xV_2O_5$ by H_2 gas. And the thickness of as-formed $Li_xV_2O_5$ layer on the LiV_3O_8 increases with the increasing of reduction time. It is noted that this surface modification strategy only involves the reduction reaction of LiV_3O_8, thus $Li_xV_2O_5$ nanolayers are promising to be more uniform than other common coating methods[24, 25]. Moreover, the intimate contact between the $Li_xV_2O_5$ layer and LiV_3O_8 core active material will benefit the improvement of cycling performance.

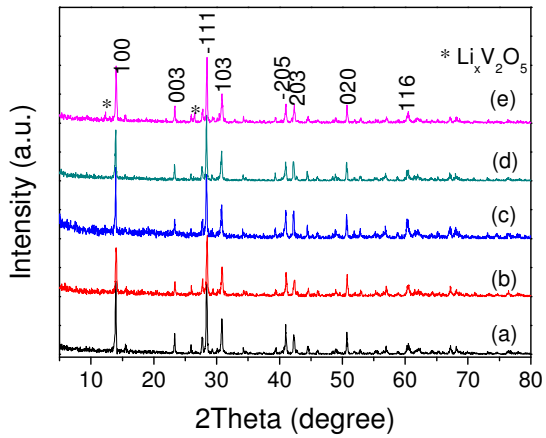

Fig. 2 XRD patterns of pristine LVO (a), LVO-1(b), LVO-5(c), LVO-10(d) and LVO-30(e)

XRD patterns of as-synthesized compounds are shown in Fig. 2. As seen, the main diffraction peaks of pristine LiV_3O_8 (LVO, a) match well with the standard monoclinic LiV_3O_8 (JCPDS Card No. 72-1193, space group: $P2_1/m$). The indexed lattice parameters of a = 0.66792 nm, b = 0.36481 nm, c = 1.22132 nm and β=108.70º are consistent with those in literature[6, 20, 30]. Apart from the diffraction peaks of monoclinic LiV_3O_8, the as-prepared sample after H_2/Ar treatment for 30 min (LVO-30, e) also indicates weak diffraction peaks at 2θ = 12.3° and 27.8°, which can be indexed into $Li_xV_2O_5$, confirming the existence of $Li_xV_2O_5$ in LVO-30. It is in good agreement with the deduction in Fig. 1 that superficial LiV_3O_8 was partially reduced to $Li_xV_2O_5$ by H_2/Ar treatment. However, such $Li_xV_2O_5$ phase is not obvious in LiV_3O_8 samples treated by shorter time (1, 5, and 10 min) using XRD. Because the reducing H_2 in the mixed atmosphere is very low (5%) and the treated time is short, it is reasonable that the slight amount of yielded $Li_xV_2O_5$ may be below the detect limitation of X-ray diffractometer. A similar phenomenon was also reported in TiN coated $Li_4Ti_5O_{12}$[31]. Thus, other precise surface analysis methods should be employed for further study.

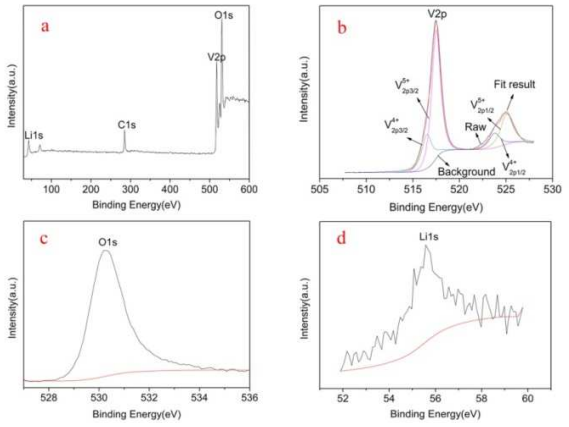

Fig. 3 XPS spectra of LVO-5: (a) survey spectrum and high-solution (b) V2p, (c) O1s, and (d) Li1s spectra.

XPS spectrum was collected for treated LiV_3O_8 to provide the further information of the surface electronic state. Fig. 3a is the XPS survey spectrum of LVO-5, in which peaks of Li1s, V2p and O1s are clearly observed. Fig. 3b is the high resolution XPS of V2p after fitting. The V^{5+}2p3/2 and V^{5+}2p1/2 peaks are centered at 517.5 and 525.2 eV, respectively, which are well consistent with the literature value for V^{5+} in LiV_3O_8 or other vanadates[28, 32]. It is noteworthy that the peaks of vanadium (+4) oxidation state are also clearly found at 516.6 (V^{4+}2p3/2) and 523.9 eV (V^{4+}2p1/2)[28, 33, 34]. Peaks at 530.5 eV (Fig. 5c) and 56.0 eV (Fig. 5d) correspond to O1s and Li1s electrons, respectively[28]. XPS results imply the existence of $Li_xV_2O_5$ on LiV_3O_8 after H_2/Ar treated LiV_3O_8 at 450 °C for 5 min, though there is no direct evidence in XRD results.

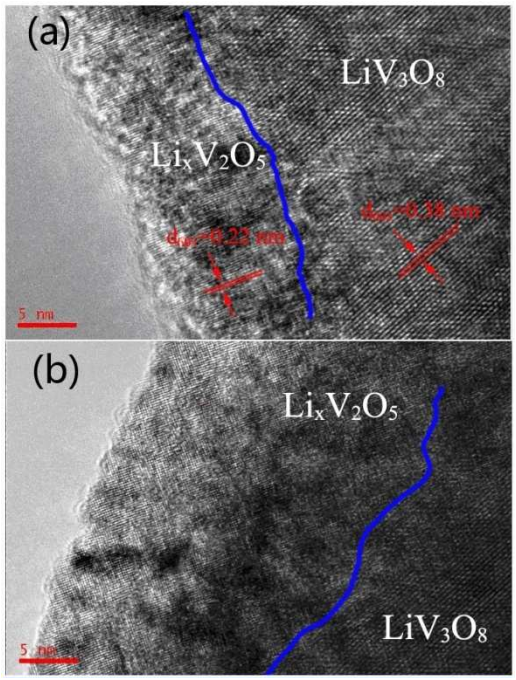

Fig. 4 HRTEM images of LVO-5 (a) and LVO-30 (b).

Fig. S1 shows the TEM images of as-prepared LVO, LVO-5, and LVO-30. All three samples are of nanoflakes morphology. However, no clear evidence for the coating could be given by the low-magnification TEM images. HRTEM images of LVO-5 (Fig. 4a) and LVO-30 (Fig. 4b) are demonstrated to provide further insights into the surface structure of as-prepared samples. As shown in Fig. 4, an obvious two-layer structure is observed for both LVO-5 and LVO-30. The periodic fringe spacing of ~0.38 nm agrees well with the interplanar spacing between {003} planes of monoclinic LiV_3O_8. Furthermore, a nanolayer with interplanar spacing of 0.22 nm exists on the surface of the LiV_3O_8 nanocrystal, corresponding to the {601} plane of $Li_xV_2O_5$. HRTEM image reveals that LiV_3O_8 nanoflakes are well coated with $Li_xV_2O_5$ layer. The thickness of $Li_xV_2O_5$ layers for LVO-5 and LVO-30 are ~12 nm and ~ 28 nm, respectively, which correspond to our designing as-proposed in Fig. 1. We have evidenced that the unique $Li_xV_2O_5/LiV_3O_8$ nanostructure could be well formed by the treatment of H_2/Ar gas.

Fig. 5 compares the CV curve of the LVO with LVO-5 at a scan rate of 0.1 $mV \cdot s^{-1}$ over the range of 1.5-4.0 V. For LVO electrode, three main anodic peaks at 2.5 V, 3.02 V, and 3.70 V

related to the extraction of Li ions, are observed. In the cathodic scan, three peaks at 2.42 V, 2.65 V, and 3.25 V are clearly observed. Peak at 2.65 V corresponds to Li ion insertion in the empty tetrahedral site through a single-phase reaction, and peak at 2.42 V is related to Li ion occupation in tetrahedral sites accompanying with a two-phase transition from $Li_3V_3O_8$ to $Li_4V_3O_8$[35]. Complicated lithium ion insertion/extraction processes are also reported for vanadates, such as LiV_3O_8[20], NaV_3O_8[32, 36], $NH_4V_3O_8$[37, 38], *etc*. For LVO-5 electrode, apart from the appearance of a new peak at 3.55 V (characteristic of $Li_xV_2O_5$)[34, 39], the main peaks also shift to left slightly. The main anodic peaks move to 2.95 V and cathodic peaks shift to 2.37 V and 2.57 V. These changes, especially the appearance of the new peak, further confirm the existence of $Li_xV_2O_5$ layer as above-discussed.

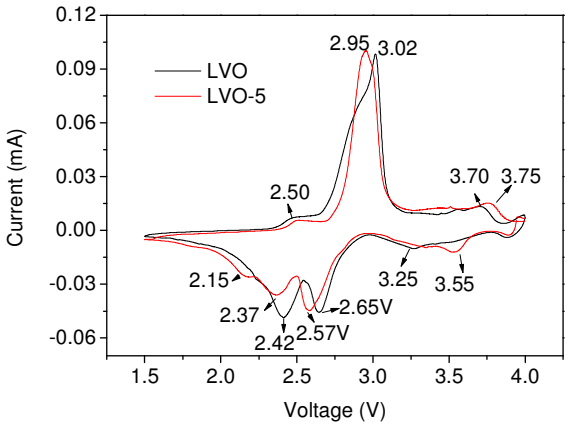

Fig. 5 CV curves of samples LVO and LVO-5 at a scan rate of 0.1 $mV \cdot s^{-1}$.

Fig. 6a gives the cycling performance of LiV_3O_8 and $Li_xV_2O_5/LiV_3O_8$ composite electrodes at 1 C rate between 1.5 and 4.0 V. The bare sample delivers a discharge capacity of 178 $mAh \cdot g^{-1}$ at the first cycle, but it sharply decreases to 145 $mAh \cdot g^{-1}$ after several cycles and 120 $mAh \cdot g^{-1}$ after 100 cycles. A quick capacity loss in initial cycles is common for bare LiV_3O_8[14, 23, 39-41]. Yang *et al.*[42] reported the LiV_3O_8 with an initial discharge capacity of 335 $mAh \cdot g^{-1}$ at 0.2 $mA \cdot cm^{-2}$, but it decreased to 240 $mAh \cdot g^{-1}$ rapidly during the first several cycles. LiV_3O_8 with an initial discharge capacity of 176 $mAh \cdot g^{-1}$ at 1C was reported by Liu *et al.* [41], however, it faded to 125 $mAh \cdot g^{-1}$ after 15 cycles. The capacity fading may arise from the dissolving of vanadium[40], irreversible phase transition between LiV_3O_8 and $Li_4V_3O_8$[43], deterioration of crystal structure[44], *etc*. After $Li_xV_2O_5$ layer formation, the cycling stability is significantly improved. The initial discharge capacity of LVO-1, LVO-5, and LVO-10 are 165.8, 195.4, and 176.4 $mAh \cdot g^{-1}$, respectively. After 200 cycles, the discharge capacities of LVO-1 and LVO-10 decrease to 151.1 and 132.0 $mAh \cdot g^{-1}$, respectively. LVO-5 exhibits the highest discharge capacity and the best cycling performance with a discharge capacity of 163.4 and 161 $mAh \cdot g^{-1}$ after 200 and 420 cycles. The corresponding capacity retention over 420 cycles is *ca.* 82%. Note that there is almost no capacity fading in the later 220 cycles for LVO-5, indicating superior cycling stability. The difference of electrochemical performance for treated LiV_3O_8 may be related to the different mass ratio of $Li_xV_2O_5$. It is known that the amount of $Li_xV_2O_5$ increases with the extension of H_2/Ar treatment. Because of the lower capacity of $Li_xV_2O_5$ compared to LiV_3O_8, it is reasonable that the reversible capacity of the composite will be affected after the surface transformation. However, as mentioned in the Introduction section, Li ion diffusion coefficient of $Li_xV_2O_5$ is several magnitudes higher than LiV_3O_8, probably leading to much improved electrode interfacial properties. Such deduction could be well approved by the improved rate performance in Fig. 7. It is believed that the

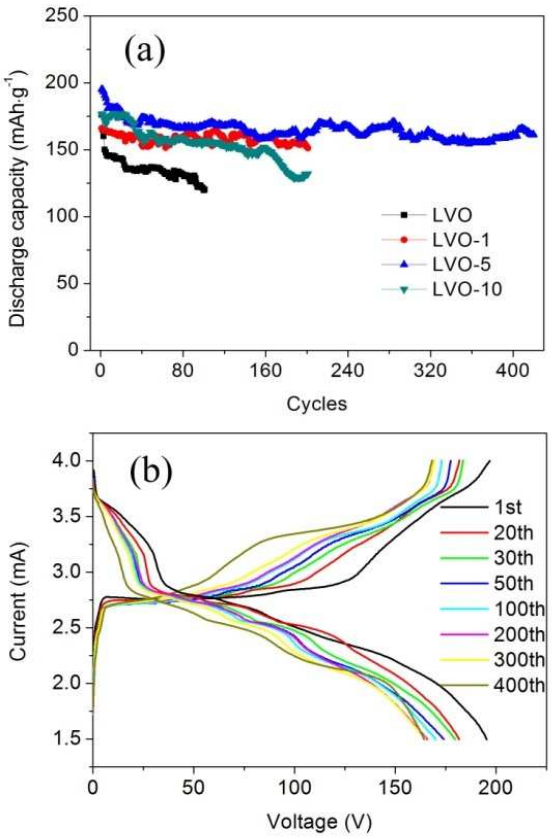

Fig. 6 (a) Cycling performance of the LVO, LVO-1, LVO-5, and LVO-10 at a current density of 300 $mA \cdot g^{-1}$ between 1.5 and 4.0 V. (b) Charge-discharge curves of LVO-5 at different cycles.

positive contribution to the reversible capacity due to the improved electrode interfacial properties would be beyond the negative effect of $Li_xV_2O_5$ introduction for the LVO-5. As the outside layer, certain $Li_xV_2O_5$ can protect the internal LiV_3O_8 well, resulting in improved cycling stability. However, too much $Li_xV_2O_5$ in the composite is unfavourable for the cycling stability. In comparison with LVO-1, the LVO-5 and LVO-10 electrodes exhibit obvious capacity loss in the first 40 cycles. Cycling performance of LVO-30, shown in Fig. S2, could further support such conclusion, which is probably due to the inferior crystal structure of $Li_xV_2O_5$. Thanks to the proper amount $Li_xV_2O_5$ layer, LVO-5 exhibits the best electrochemical properties although capacity fading in the beginning could not be neglected. The superior cycling stability here is much better in comparison with the bare LiV_3O_8[41, 45, 46] and also outperforms those surface modified LiV_3O_8, such as polypyrrole coated LiV_3O_8[47], Al_2O_3 coated LiV_3O_8[25]. Fig. 6b shows the charge-discharge curves of LVO-5 at 1C. After cycling, as seen, the plateaus from 2.7 to 2.8 V in the charge curves decrease obviously, while the plateau from 3.25 to 3.4 V exhibits an evident increase. For the discharge curves, capacity loss within the plateau from 3.3 to 3.7 V is much larger than the others. The variations of the plateaus imply possible structure self-rearrangement during the cycling.

Fig. 7(a) presents the rate performance of bare LiV_3O_8 and $Li_xV_2O_5/LiV_3O_8$ at various current densities. As shown, LVO delivers a discharge capacity of 278.7, 181.0, and 50.2 $mAh \cdot g^{-1}$ at 0.1, 1 and 5C, respectively, indicating relatively poor rate

capability. For comparison, $Li_xV_2O_5/LiV_3O_8$ samples (LVO-1, LVO-5, LVO-10) demonstrate much higher reversible capacity at various rates. LVO-5 indicates the best performance with the discharge capacities of 278.0, 195.6, 152.1, and 118.5 mAh·g^{-1} at 0.1, 1, 5 and 10 C, respectively. That is, too much $Li_xV_2O_5$ formed on LiV_3O_8 is unfavourable for reversible capacity. Note that the improved rate performance here is not only superior to bare lithium vanadate, including LiV_3O_8[25, 48] and $Li_{1.5}V_3O_8$[49], but also much better than some of carbon coated vanadates[21]. Idris *et al.* [21] fabricated carbon coated LiV_3O_8 nanosheets, which delivered a reversible capacity of 110 mAh·g^{-1} at 5C. It is worthwhile to note that our in-situ transformation strategy has advantages over carbon coating. Carbon coating will decrease the discharge capacity as well as volume energy density since the carbon is non-active. Moreover, it usually suffers from safety issue[50]. The significant improvement of rate capability for LVO-5, with no doubt, is due to the ameliorated interfacial properties of hybrid electrode because of the outside $Li_xV_2O_5$ layer. Discharge curves of LVO and LVO-5 at various rates are shown in Fig. 7b and Fig. 7c. Although the capacity at 0.1C is close, LVO-5 shows much better lithium ion insertion plateaus than LVO at the large current density.

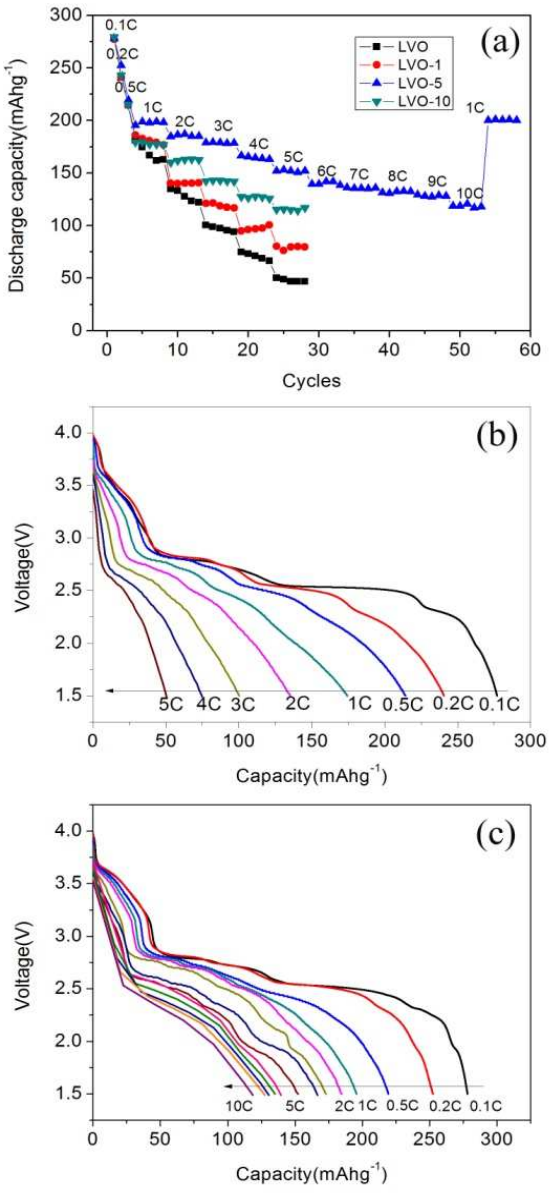

Fig. 7 (a) Rate performance of bare LiV_3O_8 and $Li_xV_2O_5/LiV_3O_8$. (b) Discharge curves of LVO from 0.1C to 5C. (c) Discharge curves of LVO-5 from 0.1C to 10C.

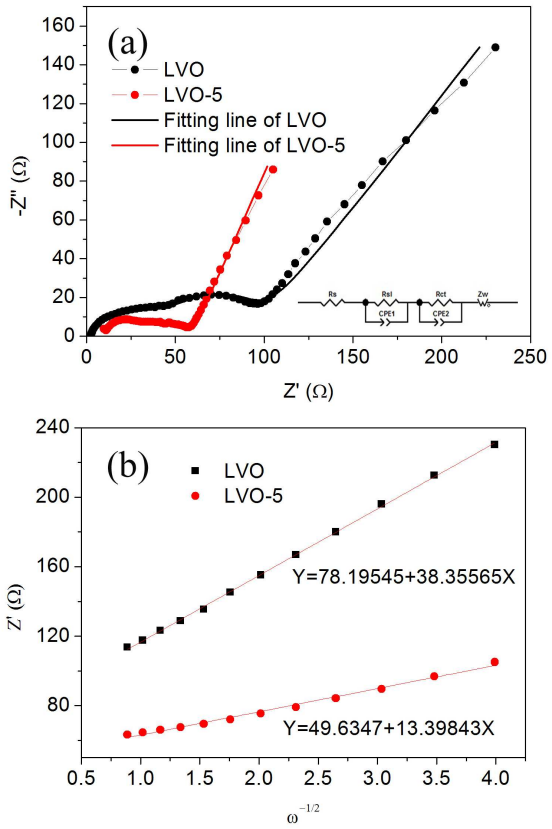

Fig. 8 Nyquist plots (a) of LVO and LVO-5 electrodes at 2.8 V and (b) the relationship curves between Z' and $\omega^{-1/2}$ in the low frequency.

The effect of $Li_xV_2O_5$ layer on the improvement of electrochemical interfacial properties was further studied by the comparison of EIS results of activated LVO with LVO-5 electrodes after several cycles. The Nyquist plots (Fig. 8) show two depressed semicircles in the high to medium frequency range. The high frequency semicircle is due to the interface parameters such as surface film contribution, porous mature of electrode, and /or the bulk of materials while the mediate semicircle is attributed to the charge-transfer resistance (R_{ct})[38, 51]. The slope line represents the Warburg impedance (Z_w) at low frequency, indicating the diffusion of Li ions in the solid matrix[38]. Obviously, the R_{ct} of the LVO-5 electrode (20 Ω) is much smaller than that of the LVO (42.5 Ω). It's well known that R_{ct} involves many factors such as electronic conductivity, crystal structure, the inter-particle contacts and electrode surface condition[52]. Accordingly, the suppressing of R_{ct}, in many previous papers, was considered as an important factor to the amelioration for electrode materials[21, 53]. Idris *et al.*[21] considered the lower R_{ct} as a reason for the better electrochemical performance of carbon coated LiV_3O_8. Sun and co-workers[53] concluded that significantly improved cycling stability of AlF_3-coated $LiCoO_2$ was attributed to the decreased R_{ct}.

Li ion diffusion coefficient could be calculated from the low frequency plots according to the following Eqs. (1) and (2). The Warburg coefficient σ_w can be obtained by Eq. (1)[38, 54].

$$Z' = R_e + R_{ct} + \sigma_w \omega^{-1/2} \quad (1)$$

Where ω (2πf) is the angular frequency in the low frequency region, both R_e and R_{ct} are kinetics parameters independent of frequency. Therefore, Z' has a linear relationship with $\omega^{-1/2}$, while the slope of the fitting line represents σ_w. Consequently, using the resulting σ_w, the diffusion coefficient (D_{Li^+}) can be calculated based on Eq. (2):

$$D_{Li^+} = \frac{R^2T^2}{2A^2n^4F^4C^2\sigma_w^2} \qquad (2)$$

In this equation, R is the gas constant, T is the temperature, A is the area of the electrode, F is the Faraday's constant, and C is the molar concentration of Li ions. Based on fitting linear equation in Fig. 8b, Li ion diffusion coefficients of LVO and LVO-5 are about 1.94×1^{-13} $cm^2\cdot s^{-1}$ and 1.59×10^{-12} $cm^2\cdot s^{-1}$, respectively. Apparently, the appearance of $Li_xV_2O_5$ layer on the LiV_3O_8 is beneficial to suppress the charge-transfer resistance and improve the Li ion diffusion coefficient, thus resulting in superior electrochemical properties.

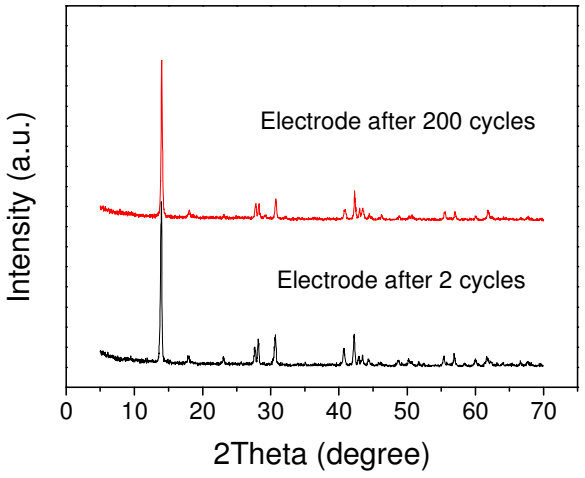

Fig. 9 XRD patterns of LVO-5 electrodes after different cycles.

XRD patterns (Fig. 9) of LVO-5 electrodes after different cycles (2, 200 cycles) are measured to evaluate the cycling stability of the $Li_xV_2O_5/LiV_3O_8$ composite. The electrode consisting of active material, carbon and binder was directly used for structure examination. XRD patterns of recovered electrodes are similar to as-prepared LVO-5 powder in Fig. 2, apart from intensity changes in some diffraction peaks. The XRD pattern of LVO-5 exhibits no visible structure change, degradation or new impurity peaks after 200 cycles compared to that after 2 cycles. The lattice parameters of LVO-5 electrodes after different cycles are further compared in Table S1. After 200 cycles, negligible change (less than 0.8%) in lattice parameters of LVO-5 electrode is demonstrated, implying good structure stability. According to the report by Jouanneau *et al.* [19], local damage of crystal structure caused by the drastic change in crystal lattice constants was an important reason for capacity fading of LiV_3O_8. Here, LVO-5 electrode possesses excellent structure stability during the cycling, in agreement with its cycling performance.

Conclusions

$Li_xV_2O_5/LiV_3O_8$ nanoflakes were successfully synthesized for the first time by a novel and facile H_2-reduction method. The uniform $Li_xV_2O_5$ layer could be well formed on the surface of LiV_3O_8 and the thickness could be controlled by the reduction time. As a result, $Li_xV_2O_5$ layer with proper thickness is highly effective in improving the electrochemical properties of LiV_3O_8. The optimized $Li_xV_2O_5$ /LiV_3O_8 nanoflakes displayed significantly enhanced cycling performance (82% of initial capacity maintaining after 420 cycles at 1C) and much better rate capability. It was evidenced that the ultrathin outside $Li_xV_2O_5$ layer could not only provide a protection for the internal LiV_3O_8, but also better the electrochemical interfacial properties, resulting in significant improvement of electrochemical performance. The self-transformation strategy here could offer a clue for surface modification of other kinds of cathode materials.

Acknowledgments

Financial support from the National Nature Science Foundation of China (No.21301193 and No.51304077), Fundamental Research Funds for the Central Universities of Central South University and Hunan Provincial Natural Science Foundation of China (No.14JJ3022 and No.13JJ4100) is greatly appreciated.

Notes and references

[a] *Key Laboratory of Resources Chemistry of Nonferrous Metals, Ministry of Education, College of Chemistry and Chemical Engineering, Central South University, Changsha, 410083, P.R China. Tel.: +86-731-88830886; Fax: +86-731-88879616. E-mail: wanghy419@126.com*

[b] *College of Chemistry and Chemical Engineering, Hunan University of Arts and Science, Changde 415000, P.R. China*

[c] *New Energy Center, National Institute of Clean-and-low-carbon Energy, Beijing, 102211, P.R China*

† Electronic Supplementary Information (ESI) available: TEM images of LVO, LVO-5, and LVO-30, Cycling performance of LVO-30 at 1C, the calculated parameters of LVO-5 electrodes after different cycles. See DOI: 10.1039/b000000x/

1. J. M. Tarascon and M. Armand, *Nature*, 2001, **414**, 359-367.
2. M. Armand and J. M. Tarascon, *Nature*, 2008, **451**, 652-657.
3. X. W. Gao, J. Z. Wang, S. L. Chou and H. K. Liu, *J. Power Sources*, **220**, 47-53.
4. X. Xiong, Z. Wang, H. Guo, X. Li, F. Wu and P. Yue, *Electrochim. Acta*, 2012, **71**, 206-212.
5. L. Liu, L. Jiao, J. Sun, Y. Zhang, M. Zhao, H. Yuan and Y. Wang, *Electrochim. Acta*, 2008, **53**, 7321-7325.
6. H. Liu, Y. Wang, K. Wang, Y. Wang and H. Zhou, *J. Power Sources*, 2009, **192**, 668-673.
7. F. Wu, L. Wang, C. Wu, Y. Bai and F. Wang, *Mater. Chem. Phys.*, 2009, **115**, 707-711.
8. J. G. Xie, J. X. Li, H. Zhan and Y. H. Zhou, *Mater. Lett.*, 2003, **57**, 2682-2687.
9. D. Wang, L. Cao, J. Huang and J. Wu, *Ceram. Int.*, **38**, 2647-2652.
10. X. Liu, J. Wang, J. Zhang and S. Yang, *J. Mater. Sci.*, 2007, **42**, 867-871.
11. L. Liu, L. Jiao, Y. Zhang, J. Sun, L. Yang, Y. Miao, H. Yuan and Y. Wang, *Mater. Chem. Phys.*, 2008, **111**, 565-569.
12. H. Y. Xu, H. Wang, Z. Q. Song, Y. W. Wang, H. Yan and M. Yoshimura, *Electrochim. Acta*, 2004, **49**, 349-353.
13. G. Yang, Y. Kong, W. H. Hou and Q. J. Yan, *J. Phys. Chem. B*, 2005, **109**, 1371-1379.
14. G. Yang, G. Wang and W. H. Hou, *J. Phys. Chem. B*, 2005, **109**, 11186-11196.
15. N. Tran, K. G. Bramnik, H. Hibst, J. Proelss, N. Mronga, M. Holzapfel, W. Scheifele and P. Novak, *J. Electrochem. Soc.*, 2008, **155**, A384-A389.
16. Y. Gu, D. Chen, X. Jiao and F. Liu, *J. Mater. Chem.*, 2006, **16**, 4361-4366.
17. M. Shui, W. Zheng, J. Shu, Q. Wang, S. Gao, D. Xu, L. Chen, L. Feng and Y. Ren, *Mater. Res. Bull.*, 2012, **47**, 2455-2459.
18. J. Kawakita, T. Miura and T. Kishi, *Solid State Ionics*, 1999, **118**, 141-147.
19. S. Jouanneau, A. L. G. La Salle, A. Verbaere and D. Guyomard, *J. Electrochem. Soc.*, 2005, **152**, A1660-A1667.
20. H. Wang, Y. Ren, Y. Wang, W. Wang and S. Liu, *CrystEngComm*, 2012, **14**, 2831-2836.

21. N. H. Idris, M. Rahman, J. Z. Wang, Z. X. Chen and H. K. Liu, *Compos. Sci. Technol.*, 2011, **71**, 343-349.
22. X. W. Gao, J. Z. Wang, S. L. Chou and H. K. Liu, *J. Power Sources*, 2012, **64**, 47-53.
23. L. Jiao, L. Liu, J. Sun, L. Yang, Y. Zhang, H. Yuan, Y. Wang and X. Zhou, *J. Phys. Chem. C*, 2008, **112**, 18249-18254.
24. H. Wang, Y. Yu, G. Jin, Y. Tang, S. Liu and D. Sun, *Solid State Ionics*, 2013, **236**, 37-42.
25. S. Huang, J. Tu, X. Jian, Y. Lu, S. Shi, X. Zhao, T. Wang, X. Wang and C. Gu, *J. Power Sources*, 2014, **245**, 698-705.
26. D. Ma, Z. Cao, H. Wang, X. Huang, L. Wang and X. Zhang, *Energy Environ. Sci.*, 2012, **5**, 8538-8542.
27. I. Zafiropoulou, M. S. Katsiotis, N. Boukos, M. A. Karakassides, S. Stephen, V. Tzitzios, M. Fardis, R. V. Vladea, S. M. Alhassan and G. Papavassiliou, *J. Phys. Chem. C*, 2013, **117**, 10135-10142.
28. W. Wang, H. Wang, S. Liu and J. Huang, *J. Solid State Electrochem.*, 2012, **16**, 2555-2561.
29. Q. Shi, R. Hu, M. Zeng and M. Zhu, *Electrochim. Acta*, 2010, **55**, 6645-6650.
30. A. Pan, J. G. Zhang, G. Cao, S. Liang, C. Wang, Z. Nie, B. W. Arey, W. Xu, D. Liu, J. Xiao, G. Li and J. Liu, *J. Mater. Chem.*, 2011, **21**, 10077-10084.
31. K. S. Park, A. Benayad, D. J. Kang and S. G. Doo, *J. Am. Chem. Soc.*, 2008, **130**, 14930-14931.
32. H. Wang, S. Liu, Y. Ren, W. Wang and A. Tang, *Energy Environ. Sci.*, 2012, **5**, 6173-6179.
33. G. Silversmit, D. Depla, H. Poelman, G. B. Marin and R. De Gryse, *J. Electron. Spectrosc. Relat. Phenom.*, 2004, **135**, 167-175.
34. L. Liu, F. Tian, X. Wang, Z. Yang and X. Wang, *Ionics*, 2013, **19**, 9-15.
35. X. Xu, Y. Z. Luo, L. Q. Mai, Y. L. Zhao, Q. Y. An, L. Xu, F. Hu, L. Zhang and Q. J. Zhang, *NPG Asia Mater.*, 2012, **4**, e20.
36. H. Wang, W. Wang, Y. Ren, K. Huang and S. Liu, *J. Power Sources*, 2012, **199**, 263-269.
37. H. Wang, Y. Ren, W. Wang, X. Huang, K. Huang, Y. Wang and S. Liu, *J. Power Sources*, 2012, **199**, 315-321.
38. H. Wang, K. Huang, Y. Ren, X. Huang, S. Liu and W. Wang, *J. Power Sources*, 2011, **196**, 9786-9791.
39. J. Liu, W. Liu, Y. Wan, S. Ji, J. Wang and Y. Zhou, *RSC Adv.*, 2012, **2**, 10470-10474.
40. S. Jouanneau, A. L. La Salle, A. Verbaere and D. Guyomard, *J. Electrochem. Soc.*, 2005, **152**, A1660-A1667.
41. Y. Liu, X. Zhou and Y. Guo, *Mater. Chem. Phys.*, 2009, **114**, 915-919.
42. G. Yang, G. Wang and W. Hou, *J. Phys. Chem. B*, 2005, **109**, 11186-11196.
43. J. Kawakita, Y. Katayama, T. Miura and T. Kishi, *Solid State Ionics*, 1998, **107**, 145-152.
44. S. Jouanneau, A. Le Gal La Salle, A. Verbaere and D. Guyomard, *J. Electrochem. Soc.*, 2005, **152**, A1660-A1667.
45. J. Xu, H. Zhang, T. Zhang, Q. Pan and Y. Gui, *J. Alloys Compd.*, 2009, **467**, 327-331.
46. Y. Feng, F. Hou and Y. Li, *J. Power Sources*, 2009, **192**, 708-713.
47. C. Q. Feng, S. Y. Chew, Z. P. Guo, J. Z. Wang and H. K. Liu, *J. Power Sources*, 2007, **174**, 1095-1099.
48. A. Sakunthala, M. Reddy, S. Selvasekarapandian, B. Chowdari and P. C. Selvin, *J. Phys. Chem. C*, 2010, **114**, 8099-8107.
49. Y. Wang, X. Xu, C. Cao, C. Shi, W. Mo and H. Zhu, *J. Power Sources*, 2013, **242**, 230-235.
50. J. Liu, S. Tang, Y. Lu, G. Cai and X. Chen, *Energy Environ. Sci.*, 2013, **6**, 2691-2697
51. Y. J. Kang, J. H. Kim, S. W. Lee and Y. K. Sun, *Electrochim. Acta*, 2005, **50**, 4784-4791.
52. J. Fan and P. S. Fedkiw, *J. Power Sources*, 1998, **72**, 165-173.
53. Y. K. Sun, J. M. Han, S. T. Myung, S. W. Lee and K. Amine, *Electrochem. Commun.*, 2006, **8**, 821-826.
54. A. Y. Shenouda and H. K. Liu, *J. Power Sources*, 2008, **185**, 1386-1391.